On the mechanism of the Antarctic Circumpolar Wave

R.J. Haarsma * F.M. Selten J.D. Opsteegh

September 28, 1999

Accepted by Journal of Climate

* *Corresponding author address:* Reindert Haarsma, Royal Netherlands Meteorological Institute, P.O. Box 201, 3730 AE De Bilt, The Netherlands, e-mail: haarsma@knmi.nl

Abstract

The variability in the subpolar Southern Hemisphere is studied with a coupled atmosphere/ocean/sea-ice model (ECBilt). After having reached an approximate statistical equilibrium in coupled mode without flux corrections, a subsequent thousand year integration is performed and analysed. A Singular Value Decomposition (SVD) of austral winter SST anomalies and 800 hPa geopotential height in the ACC region reveals a mode of covariability which resembles the observed Antarctic Circumpolar Wave (ACW). Subsequent analysis of this mode shows that it is basically an oscillation in the subsurface of the ocean. Additional experiments suggest that it is generated by the advective resonance mechanism: The oscillation is excited by the dominant modes of variability in the atmosphere, whereas the time scale is set by the ratio of the horizontal scale of these atmospheric modes and the advection velocity of the mean oceanic currents. The atmospheric response mainly consists of a local temperature adjustment to the SST anomaly which reduces the damping of the SST anomalies. Salinity, wind stress and sea-ice anomalies do modify the structure and intensity of the mode without playing an essential role.

1 Introduction

The Antarctic Circumpolar Wave (ACW) has been first discussed by White and Peterson (1996) (hereafer WP). Analysing the ECMWF analyses from 1985-94 in combination with the SST data set of Reynolds and Marisco (1993), they found an eastward propagating mode with wave number 2, circumventing the entire Antarctic ocean in about 8-10 years giving a dominant period of 4-5 years for the variation in one location. Analysis of the Topex/Poseidon measurements of anomalous surface height by Jacobs and Mitchell (1996) appeared to be consistent with the results of WP.

Similar modes of variability were found in coupled AOGCM's by Christoph et al (1998) (hereafter CBR) Cai et al (1998) and Motoi et al (1998). Some significant differences were noted however. Firstly: In CBR and Cai et al (1998) the dominant zonal wave number is three compared to two in WP. In addition WP suggest that their mode is encircling the whole Antarctic, whereas the mode of CBR has its strongest amplitude in the Pacific and is marginally existent in the southern Indian ocean. Secondly: WP found that the sea surface temperature (SST) as well as the sea level pressure (SLP) anomalies were propagating eastward and phase-locked, which strongly suggest the nature of a coupled atmosphere-ocean mode. In contrast the results of the AOGCM's show a standing SLP pattern. The results of CBR and Cai et al (1998) suggest that the standing wave pattern of the atmosphere generates SST anomalies which are advected eastward by the Antarctic Circumpolar Current (ACC). Whether these simulations represent a truly coupled mode is left as an open question in CBR, whereas Cai et al (1998) argue that the response of the standing SLP pattern to SST anomalies is an essential part of the ACW.

In support of the notion of an ocean only mode Weisse et al (1998) demonstrated the possibility of generating an ACW in an ocean model which is stochastically forced.

Bonekamp et al (1998) analysed the ECMWF reanalysis (ERA) data set. Their analyses show that during the first years of the ERA period the atmospheric mode is a standing wave pattern, whereas in the second part of the analysed period the atmosphere shows a travelling wave pattern which is phase locked with the ocean. When forcing the LSG ocean model with the ERA data set they obtained in the ocean an ACW mode similar to the ones simulated by CBR and Weisse et al (1998).

The hypothesis that the ACW is a truly coupled mode is advocated by Qiu and Jin (1997), who showed for an idealized coupled model that the fastest growing mode has the same characteristics as the ACW. Recently also Baines and Cai (1998) and Goodman and Marshall (1999) using analytical models proposed that the ACW can be considered as an unstable coupled air-sea mode.

From the discussion above it follows that the physical mechanisms responsible for the generation of the ACW are not entirely clear. Especially the question whether the ACW is a coupled mode, or an oceanic mode driven by a stochastic atmosphere, is still unresolved. In addition the oceanic processes responsible for the temporal and spatial scales of the ACW are not yet well understood.

Recently at the KNMI a coupled atmosphere-ocean-sea/ice model of intermediate complexity (ECBilt) has been developed (Opsteegh et al 1997). Because of its computational effectiveness many long integrations can be performed. Using this model we have investigated the necessary physical processes and feedback mechanisms for generating the ACW. We have done so by performing additional experiments in which a potentially important physical process has been switched on or off. This approach has been successfully used in understanding the basic mechanisms of a decadal oscillation in the North Atlantic (Selten et al 1998) (hereafter SHO). Table I summarizes the additional integrations, which will be discussed in section 3.

The specific questions we want to address are the following: 1. Is the ACW a coupled mode or can it be understood as an oceanic mode forced by the atmosphere? 2. What is the role of the ocean dynamics in the generation and maintenance of the ACW?

Section 2 gives a description of the model. The results are presented in section 3, followed by a summary and a discussion in section 4.

2 The model

2.1 Description

ECBilt is a spectral T21 global three level quasi-geostrophic model with simple parameterizations for the diabatic processes. The dynamical component of the atmospheric model was developed by Molteni (Marshall and Molteni 1993). The physical parameterisations are similar as in Held and Suarez (1978). It includes a full hydrological cycle and simple parameterisations for the long and short wave radiation. As an extension to the quasi-geostrophic equations, an estimate of the neglected ageostrophic terms in the vorticity and thermodynamic equations is included as a temporally and spatially varying forcing. This forcing is computed from the diagnostically derived vertical motion field. With the inclusion of the ageostrophic terms the model simulates the Hadley circulation qualitatively correct. This results in a drastic improvement of the strength and position of the jet stream and the transient eddy activity. Despite the inclusion of these additional terms the model is two orders of magnitude faster than AGCM's. The model is realistic in the sense that it contains the minimum amount of physics that is necessary to simulate the mid-latitude planetary and synoptic-scale circulations in the atmosphere as well as its variability on various time-scales. It is coupled to a simple coarse resolution GFDL type ocean model and a thermodynamic sea-ice model. The horizontal resolution is about 5.6×5.6 degrees, it has 12 levels in the vertical and a flat bottom. In order to increase the time step, asynchronous time stepping (Bryan, 1984) has been applied. The timestep for the atmospheric part and the sea-ice model is four hours, for the ocean it is one day. The models are synchronously coupled. For a detailed description of the atmosphere-, ocean- and sea-ice model the reader is referred to Opsteegh et al (1997), Lenderink and Haarsma (1994 and 1996) and Haarsma et al (1997). The model runs on

present generation workstations, taking 0.2 hr cpu time for the simulation of 1 yr (Power Indigo of Silicon Graphics).

2.2 Climatology

Starting from a state of rest and an idealized temperature distribution, the coupled model was integrated for 5000 years. In order to reduce a drift of increasing global temperatures and to retain a North Atlantic meridional overturning circulation some tuning was performed. Details of the spin up procedure and the climate of the last 1000 years are discussed in Opsteegh et al (1997). In this section we will summarise the climatology and variability in the Antarctic region.

In Fig. 1 we plotted the mean SST of the Southern Ocean as calculated from the 1000-year run and the observations. The calculations were based on southern hemisphere winter half-year means (MAMJJA). The model climate is warmer than observed (Levitus et al 1994), ranging from 3 K in the subtropics to about 6 K in regions close to the Antarctic continent. Especially the meridional temperature gradient at the ACC is substantially weaker. Due to the higher temperatures the amount of sea-ice simulated is much less than observed. It is mainly restricted to the Weddell and the Ross sea.

Comparing the mean and standard deviation of the 800 hPa geopotential height of the model with the NCEP reanalysis (Kalnay et al, 1996) (Fig. 2) reveals that the circumpolar vortex is considerably weaker and that also the variability is reduced. Figure 3 shows the first 4 EOFs of the 800 hPa geopotential height anomalies for the model and the NCEP reanalysis. The first EOF of both the model and the NCEP data represents a weakening and strenghtening of the polar vortex. The wavenumber 3 modulation in the NCEP data is however much less prominent in the model data. EOF 2 and 3 are reasonably well simulated.

The zonal velocity in the ACC varies between 3-4 cm/s, which is about half as observed. The subsurface velocities vary between 2-3 cm/s. In order to obtain a realistic barotropic mass transport through Drake Passage, the boundary value of the streamfunction Ψ at Antarctica was set at 100 Sv (Opsteegh et al, 1997). The relatively weak ACC despite this realistic mass transport is due to the fact that this transport is accomplished over a much thicker and broader layer than in the observations.

3 Decadal variability in the Antarctic region

3.1 Description of the mode

To explore the connection between variations in the atmosphere and the ocean, a Singular Value Decomposition (SVD, see Bretherton et al 1992) was made of the covariance structure of austral wintermean (MAMJJA) SST anomalies and 800 hPa geopotential height anomalies, denoted by Φ_{800}. An SVD analysis constructs two sets of orthogonal patterns

that optimally describe the covariance structure of two multi-variate timeseries. The patterns are ordered with respect to their singular values. The singular values measure the contribution of the corresponding pair of patterns to the total squared covariance (see Bretherton et al 1992). The first SVD pair is plotted in Fig. 4. This pair accounts for 19 % of the total squared covariance. The Φ_{800} pattern appears to be a combination of EOF 1 and EOF 3. The SST pattern projects mainly onto SST EOF 1. The variance spectrum of the SST pattern is red with significant peaks at about 8 and 16 years. The significance level was set to the 95 % a priori confidence level. The confidence limits were estimated from a Monte-Carlo simulation of 10^5 spectra of AR(1) timeseries of the same length as the analysed timeseries (1000 points). The parameters of the AR(1) process were determined from the autocorrelation coefficient at a lag of one year and the total variance of the timeseries. The variance spectrum of Φ_{800} is white, with an indication of a spectral peak at 8 years. At 16 years no enhanced variability of the Φ_{800} pattern is visible.

The third SVD mode, shown in Fig. 5, also displays significant enhanced variability of the SST pattern at a time scale of 8 years with a white spectrum for the Φ_{800} pattern. This mode accounts for 10 % of the total squared covariance. The patterns of Φ_{800} and SST project mainly on Φ_{800} EOF 4 and SST EOF 1, respectively. The second SVD mode doesn't display enhanced covariability on the decadal time scale.

In both SVD modes 1 and 3 the SST and Φ_{800} patterns are 90 degrees out of phase. This phase relationship is in agreement with the observed (WP) ACW and indicates that the warm (cold) SST anomalies are generated by anomalous warm northerly (cold southerly) winds. To check the dominant contributions to the variations in SST anomalies a budget analysis was made at 55 ^{0}S and 30 ^{0}W, which is located at the centre of the SST pattern of SVD mode 3. The dimensions of the box are 15 degrees in horizontal direction and 80 m depth. Figure 6 shows the different contributions to the variations in SST anomalies. It clearly reveals that the dominant contribution is from the anomalous heat flux, partly offset by the convection, which transports the anomalous heat to deeper layers. The direct contribution of vertical advection of heat appears to be negligible. This doesn't rule out, however, the possibility of the importance of anomalous Ekman pumping for the generation of SST anomalies as suggested by Bonekamp et al (1998). As discussed by SHO anomalous Ekman pumping destabilizes the vertical temperature gradient and thereby could enhance convection. We will return to this subject in section 3.4.

A time-longitude diagram of the ocean subsurface (averaged over 80-300m) temperature anomalies at 60 ^{o}S, shown in Fig. 7, reveals an eastward propagating signal. Maximum amplitudes of up to 2 ^{o}C are attained between 120 ^{0}W and 30 ^{0}W in the neighbourhood of Drake Passage. The subsurface advection velocity in this region deduced from Fig. 7 is about 3.5 cm/s. Eastward of it the velocity is reduced to about 1.5 cm/s. These velocities are in agreement with the simulated subsurface zonal velocities in the ACC. The eastward propagation, with the same characteristics, is also visible in time-longitude diagrams of SST anomalies (not shown), although the scatter is much larger. Comparison

with WP reveals that their SST anomalies are most intense more eastward in the Pacific sector around 150 ^{0}W and propagate much faster with an average speed of about 6-8 cm/s.

In order to identify the spatial structure of the ocean subsurface temperature signal, the method of optimal autocorrelation functions (OAF) is used. This method identifies spatial patterns of which the amplitude timeseries have an extreme autocorrelation at a specified time lag. In case of a periodically propagating signal, the OAF analysis selects at a lag of half the period two patterns of which the amplitude timeseries are in quadrature and which together describe the propagating signal. Details of the OAF technique are given in SHO. The subsurface temperature oscillation identified with the OAF analysis is shown in Fig. 8. The oscillation accounts for 13 % of the total subsurface temperature variance. The real and imaginary phase of the OAF pattern resemble the SST patterns of the third and first SVD modes, respectively. Figure 8 shows that the spectra of the two OAF patterns are nearly equal and peak at a period of about 8-9 years. The cross correlation (dashed line) peaks at a phase lag of about 2 years, the autocorrelations at about 4-5 years, which indicates that both patterns describe a propagating subsurface temperature anomaly with a period of around 8-10 years. In agreement with the time-longitude diagram (Fig. 7), the nearly equal spectra of the real and imaginary phase reveal that it is a travelling signal without a preference for one of the phases. This is also reflected by the spectral peak of 8 years in SVD 1 as well as in SVD 3, for which the SST patterns are about 90 ^{0} out of phase.

A closer look at the SST and the subsurface temperature anomaly patterns (Figs. 4, 5 and 8) reveals, that apart from the similarities, also notable differences exist, especially eastward of Drake Passage. There the subsurface temperature has a smaller zonal length scale than the SST pattern. As will be discussed in section 3.4 (see Fig. 15) due to the strong stratification there is no convective activity in the belt north-east of Drake passage between 40 ^{o}S and 55 ^{o}S. As a consequence the subsurface anomalies are decoupled from the SST anomalies. Whereas the SST anomalies are mainly forced by the anomalous sensible and latent heat fluxes induced by the Φ_{800} anomalies, the subsurface anomalies are advected with the mean current which is much reduced eastward of Drake Passage, resulting in the smaller zonal length scale. Similarly the weak convective activity south of Australia is responsible for the absence of a signal there in the OAF patterns. As an additional check on the correspondence between the SST patterns of SVD mode 1 and 3 and the subsurface OAF patterns we computed a correlation map between the time series of the two OAF patterns and SST (not shown). Apart from the regions mentioned above, the structure of the correlation maps is very similar to the SST patterns of the SVD modes (Figs. 4 and 5).

Comparing the structure of the surface patterns of this mode with the observed ACW mode by WP, we conclude that a strong resemblance exists between those modes, like the eastward propagation of the SST anomalies and the phase relationship between SLP and SST patterns. One of the main differences is that the mode of ECBilt displays

a smaller spatial scale with predominantly wave number 3, whereas the mode of WP has wave number 2. We note, however, that the ACW modes simulated by CBR and Cai et al (1998) in AOGCM's and by Bonekamp et al (1998) in an OGCM with observed surface fluxes also display a somewhat smaller zonal spatial scale with patterns dominated by wavenumbers 2 and 3. Also by analysing the ECMWF and NCEP reanalysis data sets Connolley (1998) observed the appearence of both wave number 2 and 3 patterns. Another difference is that the ACW mode by WP has its strongest signal in the Pacific sector, whereas in ECBilt the maximum amplitudes are shifted more westward to the neighbourhood of Drake passage. The longer time scale of 8 years instead of the observed 4 years is due, as will be shown in section 3.3, to the weaker than observed ACC in ECBilt.

The importance of ENSO for generating the ACW is still under debate. Although observational studies by WP and Peterson and White (1998) suggest a connection between ENSO and the ACW, the AOGCM's used by CBR and Cai et al (1998) don't reveal this link, despite the fact that they do simulate ENSO like variability. ECBilt does not generate ENSO type of variability, probably due to its coarse resolution and the use of quasi-geostrophic dynamics for the simulation of the atmospheric circulation. The fact that ECBilt does generate an ACW mode is therefore in agreement with the results of other AOGCM's. This, however, doesn't rule out the possibility of the role of ENSO in phase locking and amplifying the ACW.

In conclusion we argue that despite the significant differences, the observed ACW and the mode in ECBilt are qualitatively the same and that a detailed analysis of the mode in ECBilt will shed light on the basic physical mechanisms responsible for the generation and maintenance of the observed ACW. In the remainder of this article we will therefore call it the ACW in ECBilt.

3.2 Is it a coupled mode?

WP and Qiu and Jin (1997) hypothezise that the ACW is a coupled pheneomenon. The Φ_{800} anomalies might be reinforced by upstream SST anomalies. Elaborating on this idea Qiu and Jin (1997) showed in an idealized model that for a certain choice of parameters this feedback mechanism results in an unstable growing mode. Different mechanisms for generating a coupled ACW are proposed by Cai et al (1998) and Goodman and Marshall(1999). On the other hand the analyses of Weisse et al (1998) and Bonekamp et al (1998) strongly advocate the idea that the ACW is forced by the atmosphere and that the main role of the ocean is setting the time scale.

One of the arguments of WP in favour of a coupled mode is the phase locking of SST and SLP anomalies. However, as mentioned in the introduction, Bonekamp et al (1998) by analyzing the ERA data set conclude that this is only true for certain periods, whereas in other periods there is no sign of coherent propagation of SST and SLP anomalies. The same conclusion was also reached by Connolly (1998). The time-longitude diagram at 60 ^{0}S, shown in Fig. 9, reveals that in ECBilt there is no indication of coherent eastward

propagation of Φ_{800} anomalies. It might be that the explained variance of the propagating anomalies is too small to be detected on the time-longitude diagram. We therefore projected the Φ_{800} anomalies on the Φ_{800} patterns of SVD modes 1 and 3 before constructing the time-longitude diagram. This time-longitude diagram (not shown) also doesn't display propagating anomalies.

It was pointed out by Cai et al (1998) that the absence of phase-locking does not necessarely imply that it is not a coupled mode. They show that the interaction between standing SLP waves and propagating SST anomalies can generate a coupled mode of variability. To investigate further whether or not the atmospheric response to SST anomalies is essential for the ACW in ECBilt, we therefore performed the following experiment. We repeated the 1000-year coupled integration but on an arbitrary year (year 37) we decoupled the atmosphere from the ocean. From that year onwards, we used the daily SST values and sea-ice cover of that year as the lower boundary condition for the atmosphere. The ocean and sea-ice are forced by the varying atmosphere. So the ocean is forced with fluxes, that depend on the actual SST values, whereas the surface heat fluxes that the atmosphere receives depend on the prescribed SST's. We will denote this one-sided coupled experiment by OC and the fully coupled experiment by C. From year 100 to 1100, we calculated the SVD of the covariance between SST and Φ_{800} anomalies.

The patterns of the first SVD pair are very similar to those of the first SVD pair of the coupled run. Also the patterns of the second SVD pair in the OC run are very similar to the patterns of the third SVD pair in the C run. This implies that the structure of the SVD pairs in the C run is largely the result of the atmosphere forcing the ocean. Because the difference in the explained covariance of the second and third SVD pair is small (12 and 10 %) the reversed order in SVD pairs is not relevant and may partly be due to limited sampling. Inspection of the variance spectra of the SVD pairs in the OC run reveals that the spectral peaks at 8-9 years have disappeared. What remains are virtually red spectra for the SST modes and white spectra for the Φ_{800} modes. Furthermore, the SST variance is less red. The variance at long timescales has dropped to about 50 % compared to the C run. The SST variance being less red is due to the fact that forcing the ocean with specified SAT, as in the OC run, implies an atmosphere with an infinite heat capacity, whereas in the fully coupled run the fluxes are moderated by the atmosphere's finite heat capacity (Saravanan, 1998). As a consequence in the OC run the SST are strongly relaxed to SAT with a time constant in the order of a month. Because the SAT spectrum in the C run, as an atmospheric variable, is more white than the SST spectrum this results in a SST spectrum in the OC run which is more white than in the C run.

At first sight the disappearance of the spectral peaks in the SST seems to indicate that the weak response of the atmospheric circulation to SST anomalies is indeed essential for the decadal oscillation in the model. However, an OAF analysis of the subsurface temperature in the OC run, with patterns shown in Fig. 10, reveals that the subsurface oscillation is still present. The changes in the structure are small, but comparison of the variance spectra of the OC run, shown in Fig. 10c, with those of the coupled run reveals

that the variance is drastically reduced by a factor of three.

Because the subsurface oscillation, although much weaker, is still present in the one-sided coupled experiment, with the same preferred time scale and the same structure, we must conclude that the coupling is not essential for generating the structure and the time scale of the ACW mode in ECBilt.

From this experiment it is, however, not yet clear whether this mode is due to stochastic forcing or whether it is generated by purely internal ocean dynamics. In order to test the latter hypothesis, we forced the ocean model with heat fluxes and windstress fluxes following a fixed annual cycle. These fluxes were computed by averaging the daily fluxes during the first hundred years of the coupled integration. After year 37 of the coupled integration these fluxes were used to force the ocean model during a period of 150 years. We will call this experiment FA. In the FA experiment the ACW rapidly dies within a few years. Apart from the annual cycle the thermal and salinity structure of the upper Southern Ocean does not reveal any significant variability. It is therefore the stochastic forcing which generates the ACW mode in ECBilt.

The coupling of the atmosphere with the ocean is, however, very important for the strength of the mode and its signal at the surface. The same conclusion was reached by SHO for a decadal oscillation in the North Atlantic. Atmosphere only experiments in SHO revealed that there is a strong thermodynamic response to SST anomalies, by which the surface air temperature (SAT) adjusts to SST anomalies thereby strongly reducing the atmosphere-ocean fluxes, which tend to damp the SST anomalies. Thus once an SST anomaly is generated it is weakly damped by the atmosphere in the C run. In the OC run this damping is overestimated, because the SAT is not allowed to vary, which explains the absence of the spectral peak.

We investigated the atmospheric response to SST anomalies in the Southern Ocean with atmosphere only experiments. In these experiments we took as SST anomalies the SST patterns of SVD modes 1 and 3 and integrated the atmospheric model for 100 years. Likewise as in SHO the main response is a thermodynamic response, which reduces the damping of the SST anomalies. In addition also a dynamic response in the Φ_{800} field is generated, with a high (low) down stream of a warm (cold) pool. If strong enough this response would reinforce the SST anomaly. The amplitude of this response, however, is rather weak, about 30 % of the standard deviation of the control run. These results, together with the absence of a clear spectral peak in the Φ_{800} spectra of SVD modes 1 and 2, and the continued existence of the ACW in the one-sided coupled run indicate that the dynamic atmospheric response to SST anomalies is not essential for the generation of the ACW in ECBilt.

3.3 Advective resonance hypothesis

A theory which explains the existence of a preferred time scale in the ocean when it is stochastically forced by the atmosphere is the advective resonance hypothesis by Sara-

vanan and McWilliams (1998). According to this hypothesis a stochastic atmosphere with spatial scale L forcing an ocean with characteristic velocity scale V, generates a preferred mode with a time scale L/V in the ocean. For the wavenumber three mode at 60 ^{0}S this would require for a dominant time scale of 8 years an ocean velocity of about 2.5 cm/s, which is roughly in agreement with the surface ocean velocities in the ACC in ECBilt.

In order to test whether indeed the ocean velocity determines the time scale, we did a 325 year time integration in which we increased the barotropic part of the Antarctic Circumpolar Current from 100 Sv to 500 Sv. This was done by increasing the boundary value of the streamfunction Ψ at Antarctica (Opsteegh et al, 1997). This run is referred to as C+. As a result the zonal surface currents are increased with about a factor of two. The SVD analysis of SST and Φ_{800} now shows a mode with a dominant time scale of 4 years, half the time scale in the C run. The OAF analysis also reveals a subsurface oscillation with a period of about four years. Figure 11 shows that, compared to the C run, the oscillation extends much farther to the east of Drake Passage, involving two wave lengths instead of one. The mode, generated in the area around Drake Passage, can travel twice as far within the same damping time scale.

A prerequisite for the advective resonance hypothesis is that an ocean temperature anomaly can survive long enough in order to be reinforced by the atmospheric forcing. We investigated the diffusion of the anomaly due to oceanic processes by means of a passive tracer experiment. Starting with an initial distribution in the shape of one of the OAF modes it appears that after about 4 years it has travelled half a wavelength and that its amplitude is reduced by about 50%. In the advective resonance hypothesis the oceanic temperature anomaly has to travel half a wavelength in order to be reinforced by the opposite phase of the standing atmospheric pattern. Thus from this passive tracer experiment we can conclude that the advective resonance hypothesis is a possible candidate for explaining the ACW mode simulated in ECBilt.

Finally we checked whether, as in the advective resonance hypothesis, the ocean indeed can be considered passive with a constant (in time) advection velocity V. We therefore did the following experiment: We repeated the 1000 year integration, but from year 37 onwards we used the daily ocean velocities u,v and w at all levels of that year to advect salinity and temperature anomalies. This mimicks the example of Saravanan and McWilliams (1998) of an ocean with constant V. We will denote this fixed ocean run by FO. Again the same SVD pairs of SST and Φ_{800} anomalies as in the C run are found. However, the spectral peaks have disappeared and the SST variance at long time scales has decreased with about 40% with respect to the control run. The OAF analysis as well as the time-longitude diagrams of the subsurface temperature anomalies reveal that the subsurface oscillation is still present, although somewhat weaker, but with the same time scale. The OAF patterns of the real and imaginary phase are very similar to the ones of the coupled integration, but the variance is about 50 % weaker. In order to investigate the reduced strength of the subsurface oscillation in the FO run, we made a correlation map between the amplitude of the real phase of the OAF pattern and the temperature in the

zonal-depth plane at 60 ^{0}S. Figure 12 shows that in the FO run the signal penetrates to smaller depths compared to the C run, which reduces the heat storage associated with the anomalies. In the stochastic climate model of Hasselmann (1976), an ocean with larger heat capacity that integrates the atmospheric forcing leads to larger SST variability on longer time scales. In subsequent paragraphs we will show that both salinity anomalies and Ekman pumping due to wind stress anomalies contribute to the deepening of SST anomalies. These processes are absent in the FO run. Summarizing we conclude from this experiment that the advective resonance hypothesis appears to be a plausible explanation for the existence of the ACW mode, although other processes affect its structure and strength, but not the time scale. This will be the subject of the following paragraphs.

3.4 Role of salinity, wind stress and sea-ice

Salinity

Correlation maps of the timeseries of the subsurface temperature OAF patterns with the surface salinity in the C run, shown in Fig. 13, reveal that subsurface temperature variations are accompanied by surface salinity variations. Maximum correlations of about 0.4 are attained just north-west of Drake Passage, while the South Atlantic ocean shows correlations up to 0.6. A budget analysis in a surface box of 15 by 15 degrees centered around 50 ^{o}S and 90 ^{o}W, located at the largest upstream salinity variations, reveals that the dominant term is the horizontal advection of salinity with a smaller contribution from convection. Vertical advection appears to be negligible. The salinity variations are generated by the anomalous near geostrophic currents around the warm and cold pools. The anomalous subsurface currents related to the ACW mode are plotted for half a period in Fig. 14, showing the cyclonic circulation around anomalous warm pools and vice versa. In the presence of a strong horizontal salinity gradient these anomalous currents will induce relatively large salinity anomalies, which in case of marginal stability will then modify the convective activity. Indeed Fig. 15 shows that the positive salinity anomalies significantly enhance the convection around 50 ^{o}S and 90 ^{o}W. However, Fig. 15 also shows that in case of strong stable stratification, like in the region east of the coast of South America, convection will not be triggered. Indeed a budget analysis in a surface box of 15 by 15 degrees centered around 40 ^{o}S and 40 ^{o}W, reveals that there convection is negligible and that the salinity variations are almost solely due to horizontal advection.

In SHO it was found that variations in convective activity due to salinity fluctuations play a crucial role in the North Atlantic decadal mode simulated by ECBilt. However, the existence of the ACW mode in the FO run, where the horizontal advection of salinity by the anomalous currents is by definition zero, indicates that generation of salinity anomalies by anomalous advection is not essential. A closer look at the differences in the OAF patterns between the C and FO run (not shown) reveals that in the region of largest variations in convective activity induced by salinity anomalies, the signal has disappeared

in the FO run, in agreement with our expectations.

In Lenderink and Haarsma (1994) it was shown that salinity can also lead to so-called sustained convection, which is maintained by a positive salinity feedback. As an additional check on the role of salinity we did therefore the same experiment as in SHO. A coupled integration was started and in the first 100 years the climatological annual cycle of salinity in each grid box was calculated. From year 100 onwards, salinity was treated as a passive tracer. In the calculation of the density, the daily climatological values were used instead of the actual salinity values. Thus the salinity anomalies do not influence the ocean velocities and convective activity. This run is referred to as CS run. The model displayed a significant climate drift after making the salinity a passive tracer. Especially the sea ice coverage underwent large changes, with a reduction of the ice area of about 30 %. This is accompanied by an increase of the surface temperature in the Antarctic ocean of about 0.3 ^{o}C. In addition to the climate drift a large temperature oscillation of about 250 years develops extending from the surface to the bottom. On this oscillation a higher frequency mode of about 40 years is superimposed. The cause of the climate drift and the oscillations are unknown and fall outside the scope of this paper. However, the ACW still exists notwithstanding the large climate drift and the low-frequency oscillation. An OAF analysis on 15 year highpass filtered subsurface temperature data reveals on a time scale of about 8 years a mode with very much the same structure as in the C run. Similarly as in the FO run the signal has disappeared in the regions of salinity induced convective activity. The variability of the mode is reduced with about a factor of two. Thus salinity anomalies are not essential for the mode, but modify the structure and the variance.

Wind stress

In section 3.1 we mentioned that the vertical advection of temperature in the heat budget is negligible, but we raised the point that the vertical velocities induced by wind stress anomalies might influence the convective activity. An SVD analyses of Φ_{800} and the vertical velocity at 300 m depth (not shown) in the C run reveals that the dominant modes of variability in Φ_{800} covary with distinct patterns of anomalous upwelling and downwelling. During the austral winter the surface of the ocean is cooled by the atmosphere. The surface cooling is partly compensated by convection, which mixes warmer water from below to the surface. Anomalous strong (weak) upwelling will bring more (less) dense water to the surface, thereby increasing (decreasing) the convection. In order to investigate how the anomalous upwelling affect the ACW mode in ECBilt we repeated the 1000 year integration but from year 37 onwards we forced the ocean by the daily wind stresses of that year, keeping everything else the same as in the C run. In the calculation of the sensible and latent heat fluxes the actual winds were used. This run will be referred to as CW run. The structure of the SVD modes remains largely the same with a reduced amplitude of the SST pattern at lower frequencies. The peaks at 8 and 16 year in the

spectrum of the first mode of SST have disapeared while the peak at 8 years in the third mode of SST is also somewhat reduced. The OAF analyses again shows a dominant mode in the subsurface temperatures with a period of 8 years, for which the patterns are almost exactly the same as in the C run. The amplitude is, however, reduced with about 40 %, the reason being that the temperature anomalies are less deep in the CW run.

Sea-ice

The SST patterns of the SVD modes as well as the OAF patterns of the subsurface temperature oscillation show their maximum amplitudes well away from the sea-ice covered areas. This indicates a minor role for sea-ice in generating the ACW mode in ECBilt. This is further confirmed by the relatively low correlations of order 0.2 between the time series of the OAF patterns of the subsurface temperature and the sea-ice coverage. In order to confirm whether indeed sea-ice is of minor importance for the ACW mode we did another 1000 year run in which we prescribed the annual cycle of the sea-ice coverage (CI run). This annual cycle was computed by averaging the daily values of the sea-ice coverage in the first 100 years of the integration. The OAF analysis of the subsurface temperature, shown in Fig. 16, reveals a mode with a structure which is significantly reduced in the Pacific Ocean, south of 60 ^{o}S. Probably sea-ice fluctuations in the Ross sea affect the structure of the ACW mode down stream. Most variance is now found at a somewhat longer time scale of about 11 years in accordance with the smaller velocities in the ACC at greater distance from the Antarctic continent. The amplitude of the mode is reduced with about 50 %. The reason is unclear. It might be due to the neglected interaction between sea-ice and convection or a change in the mean stratification due to the climate drift.

From these experiments we conclude that salinity, wind stress and sea-ice fluctuations are not crucial for the generation and further evolution of the ACW mode in ECBilt. They, however, are important for the strength and the details of the structure of the mode.

4 Summary and discussion

The coupled integration of ECBilt simulates a mode of variability in the Antarctic regions which bears qualitatively strong simularities with the ACW described by WP. Because of its computational efficiency, additional experiments are possible to unravel the cause and effect relationships. The Antarctic mode simulated by ECBilt is basically an oscillation in the interior of the ocean which is excited by preferred patterns of variability of the atmosphere. The atmospheric response mainly consists of a local surface temperature adjustment to the SST anomaly which reduces the damping of the SST anomalies. The advective resonance hypothesis of Saravanan and McWilliams (1998), which assumes that the ocean passively advects SST anomalies that are generated by atmospheric cir-

culation anomalies is the most plausible explanation of the simulated mode of variability. Other phenomena like salinity anomalies generated by anomalous surface currents, anomalous Ekman pumping induced by wind stress anomalies and anomalous sea-ice coverage strengthen and modify the mode but are not essential for the structure and preferred time scale. The dominant modes of variability in the atmosphere imprint their structure on the ocean. The preferred timescale is set by the ratio of the spatial scale of these dominant modes and the characteristic ocean velocity of the ACC.

We did not find evidence that the Antarctic mode simulated by ECBilt is an unstable coupled mode. ECBilt is a climate model of intermediate complexity. One could argue that due to the coarse resolution and the relatively simple representation of the physical processes, ECBilt underestimates the coupling between atmosphere and ocean. However, the fact that the model simulates a mode which qualitatively resembles the observed ACW, suggests that ECBilt captures the essential elements for the generation of this mode.

An alternative view point is offered by W.B. White (personal communication) who argues that the longer time scale of the mode in ECBilt compared with the observed ACW indicates that the model doesn't simulate the observed ACW but a 'stochastic ACW like' mode. This is based on the argument that the time scale of a coupled ACW mode computed by White et al (1998) from an analytical model appears to be shorter than the advective time scale. Also in re-analyzing the data of CBR W.B. White (personal communication) argues that in 20% of the data an exact ACW exists but that in the remaing 80% the stochastic wave of CBR prevails.

The integrations done with ECBilt have been used in an earlier study (SHO) on a decadal mode in the North Atlantic, which bears strong similarities with the observed North-Atlantic decadal mode. Both the model equivalences of the observed ACW and the North-Atlantic decadal mode can be understood as modes which are generated by a stochastic atmosphere with preferred spatial scales, with the ocean setting the preferred time scale. It therefore appeares that this is a generic mechanism for midlatitude decadal variability. The main difference between the ACW and the NAO mode in ECBilt is the role of the ocean. In the NAO mode salinity anomalies appear to play a decisive role, whereas the ACW mode in ECBilt is generated by the advective resonance mechanism of Saravanan and McWilliams (1998) with salinity anomalies playing only a modifying role.

Acknowledgements

Selten was supported by the Dutch National Research Programme on Global Air Pollution and Climate Change, registered under nr. 951208, titled: "Climate Variability on Decadal Timescales". We thank Hans Bonekamp, Andreas Sterl, Saravanan and an anonymous reviewer for their valuable comments on the first draft of this paper.

References

Baines, P.G. and W.J. Cai, 1998: An interactive instability mechanism for the Antarctic Circumpolar Wave. Submitted to J. Climate.

Bonekamp, H., A. Sterl and G. Komen, 1998: Interannual variability in the Southern Ocean from an OGCM forced by ECMWF re-analysis fluxes. Accepted by J. Geophys. Res.

Bretherton, C.S., C. Smith and J.M. Wallace, 1992: An intercomparison of methods for finding coupled patterns in climate data. J. Climate, 5, 541-560.

Bryan, K., 1984: Accelerating the converge to equilibrium of ocean climate models. J. Phys. Oceanogr., 14, 666-673.

Cai, W., P.G. Baines and H.B. Gordon, 1998: Southern mid-to-high latitude variability, a zonal wavenumber 3 pattern, and the Antarctic Circumpolar Wave in a coupled model. Submitted to J. Climate.

Christoph, M. T.P. Barnett and E. Roeckner, 1998: The Antarctic circumpolar wave in a coupled ocean-atmosphere GCM. J. Climate, 11, 1659-1672.

Connolley, W.M., 1998: A closer look at the Antarctic Circumpolar Wave. Submitted to Clim. Dyn.

Goodman, J. and J. Marshall, 1999: A model of decadal middle-latitude atmosphere-ocean coupled mode. J.Climate, 12, 621-641.

Haarsma, R.J., F.M. Selten. J.D. Opsteegh, G. Lenderink and Q. Liu, 1997: ECBILT: A coupled atmosphere ocean sea-ice model for climate predictability studies. KNMI technical report TR-195, De Bilt, The Netherlands.

Hasselmann, K., 1976: Stochastic climate models. Part I. Theory. Tellus, 28, 473-485.

Held, I.M. and J.M. Suarez, 1978: A two level primitive equation atmosphere model designed for climate sensitivity experiments. J. Atmos. Sci., 35, 206-229.

Jacobs, G.A. and J.L. Mitchell, 1996: Ocean circulation variations associated with the Antarctic Circumpolar Wave. Geophys. Res. Let., 23, 2947-2950.

Kalnay, E., M. Kanamitsu, R. Kistler, W. Collins, D. Deaver, L. Gandin, M. Iredell, S. Saha, G. White, J. Woollen, Y. Zhu, A. Leetma, R. Reynolds, M. Chelliah, W. Ebisuzaki, W. Higgins, J. Janowiak, K.C. Mo, C. Ropelewski, J. Wang, R. Jenne, 1996: The NCEP/NCAR 40-year reanalysis project. Bull. Am. Met. Soc., March 1996.

Lenderink, G. and R.J. Haarsma, 1994: Variability and multiple equilibria of the thermohaline circulation associated with deep water formation. J. Phys. Oceanogr., 24, 1480-1493.

Lenderink, G. and R.J. Haarsma, 1996: Rapid convective transitions in the presence of sea-ice. J. Phys. Oceanogr., 26, 1448-1467.

Levitus, S., A.M. Da Silva and C.C. Young, 1994: Atlas of surface marine data 1994, Volume 2: Anomalies of directly observed quantities. National Oceanographic Data Center, User Services Branch, NOAA/NESDIS E/OC21, 1825 Connecticut Avenue, NW Washington, DC20235, USA, 416pp.

Marshall, J. and F. Molteni, 1993: Toward a dynamic understanding of planetary-scale flow regimes. J. Atmos. Sci., 50, 1792-1818.

Motoi, T., A. Kito and H. Koide, 1998: Antarctic circumpolar wave in a coupled ocean atmosphere model. Annals Glaciology, in press.

Opsteegh, J.D., R.J. Haarsma and F.M. Selten, 1997: ECBILT a suitable alternative to mixed boundary conditions in ocean models. Tellus, 50A, 348-367.

Peterson, R.G. and W. B. White, 1998: Slow oceanic teleconnections linking the Antarctic Circumpolar Wave with the tropical El Nino-Southern Oscillation. Journ. Geophys. Res., 103, 24573-24583.

Qiu, B. and F.F. Jin, 1997: Antarctic circumpolar waves: An indication of ocean-atmosphere coupling in the extratropics. Geophys. Res. Lett., 24, 2585-2588.

Reynolds, R.W. and D.C. Marisco, 1993: An improved real-time global sea surface temperature analysis. J. Climate, 6, 114-119.

Saravanan, R. and J. C. McWilliams, 1998: Advective ocean atmosphere interaction: an analytical stochastic model with implications for decadal variability. J. Climate, 11, 165-188.

Selten, F.M., R.J. Haarsma and J.D. Opsteegh, 1998: On the mechanism of North Atlantic decadal variability. J. Climate. In press.

Weisse, R., U. Mikolajewicz, A. Sterl and S.S. Drijfhout, 1998: Stochastically forced variability in the Antarctic circumpolar current. Accepted by J. Geophys. Res.

White, B.W and R.G. Peterson, 1996: An Antarctic circumpolar wave in surface pressure, wind, temperature and sea-ice extent. Nature, 380, 699-702.

White, B.W, Shyh-Chin Chen and R.G. Peterson, 1998: The antarctic circumpolar wave: A beta effect in ocean-atmosphere coupling over the southern ocean. J. Phys. Oceanogr., 28, 2345-2361.

Table Captions

Table I: Overview of the integrations

Figure Captions

Figure 1: Southern hemisphere winter half-year mean (MAMJJA) SST of the 1000-year coupled integration (a) and of the Levitus (1994) data (b).

Figure 2: Southern hemisphere winter half-year mean (MAMJJA) geopotential height and the standard deviation of daily geopotential height values [gpdm], both for the 1000-year coupled integration at 800 hPa (a,c) and the NCEP-NCAR data at 850 hPa (b,d) (global mean subtracted).

Figure 3: Patterns of EOF 1-4 and the associated variance of the NCEP-NCAR reanalyses Φ_{800} data (a) and of the 1000-year coupled integration (b).

Figure 4: First SVD mode of the Southern hemisphere wintermean (MAMJJA) SST and Φ_{800} anomalies for the 1000-year coupled integration: (a) pattern Φ_{800} [gpdm], (b) pattern SST [^{o}C], (c) variance spectrum SST and (d) variance spectrum Φ_{800} with red noise fit and 95% confidence interval. The spatial patterns are scaled such that the values correspond to one standard deviation.

Figure 5: Third SVD mode of the Southern hemisphere wintermean (MAMJJA) SST and Φ_{800} anomalies for 1000-year coupled integration: (a) pattern Φ_{800} [gpdm], (b) pattern SST [^{o}C], (c) variance spectrum SST and (d) variance spectrum Φ_{800} with red noise fit and 95% confidence interval. The spatial patterns are scaled such that the values correspond to one standard deviation.

Figure 6: Budget analysis of year to year changes in SST anomalies in a 15 by 15 degrees surface box (upper 80m) centered at 55 ^{o}S and 30 ^{o}W. The solid line corresponds to temperature tendency, the long dashed line corresponds to net surface heat flux plus convection, the short dashed line corresponds to horizontal advection of heat and the dotted line corresponds to vertical advection of heat.

Figure 7: Time-longitude diagram of the ocean subsurface (80-300m) temperature anomalies [^{o}C] along 60 ^{o}S.

Figure 8: Subsurface temperature oscillation as identified by OAF modes at lag 4 years: (a) real phase, (b) imaginary phase, (c) variance spectrum real phase and imaginary phase, (d) auto correlation of the real phase (solid), imaginary phase (dotted) and the cross correlation (dashed). The spatial patterns are scaled such that the values correspond to one standard deviation [^{o}C].

Figure 9: Time-longitude diagram of Φ_{800} [gpdm] anomalies along 60 ^{o}S.

Figure 10: As figure 8, but now for the one-sided coupled run (OC run).

Figure 11: As figure 8, but now for the run in which the barotropic component of the ACC has been increased from 100 Sv to 500 Sv (C+ run).

Figure 12: Correlation map between the amplitude of the OAF pattern of the real phase and the temperature in the zonal plane between 200 ^oW and 60 ^oE at 60 ^oS in the FO run (a) and the C run (b).

Figure 13: Correlation map between the amplitude of the OAF modes and the surface salinity in the C run.

Figure 14: Timeseries of subsurface (80-300m) temperature [K] anomalies projected onto the OAF patterns describing the ACW mode of ECBilt. Arrows denote the anomalous subsurface currents [m/s], also projected onto the corresponding OAF patterns. First plot corresponds to year 285 of the C run. Time step between the plots is one year.

Figure 15: Correlation map between the amplitude of the OAF patterns and the strength of the convection in the C run.

Figure 16: As figure 8, but now for the run with climatological sea-ice coverage (CI run).

Name	Description
C	Coupled integration
OC	One-sided coupling
FA	Fixed atmosphere
C+	Stronger ACC
FO	Fixed ocean velocities
CS	Constant salinity
CW	Constant wind stress
CI	Climatological sea ice cover

Table I

a

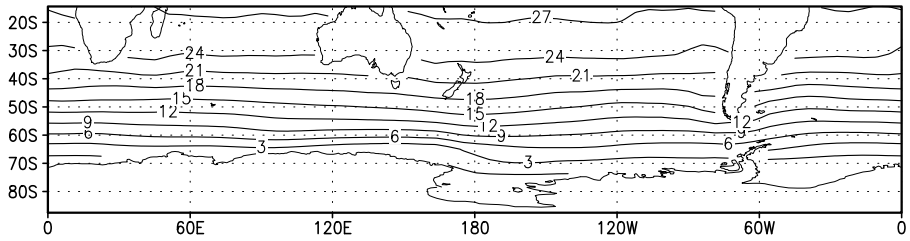
20S
30S
40S
50S
60S
70S
80S
0
60E
120E
180
120W
60W
0
27
24
21
18
15
12
9
6
3

b

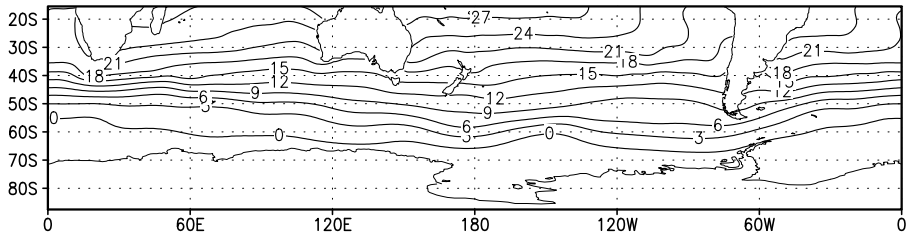
20S
30S
40S
50S
60S
70S
80S
0
60E
120E
180
120W
60W
0
27
24
21
18
15
12
9
6
3
0

Figure 1

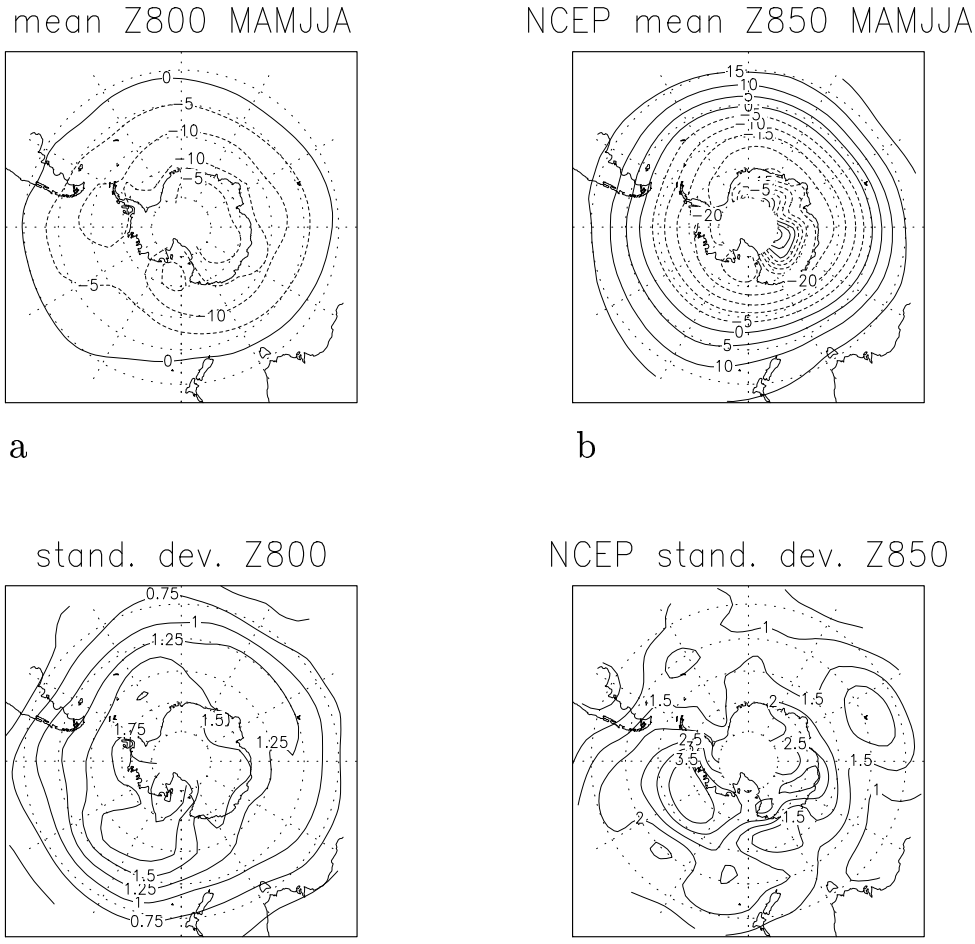
mean Z800 MAMJJA
NCEP mean Z850 MAMJJA
a
b
stand. dev. Z800
NCEP stand. dev. Z850
c
d

Figure 2

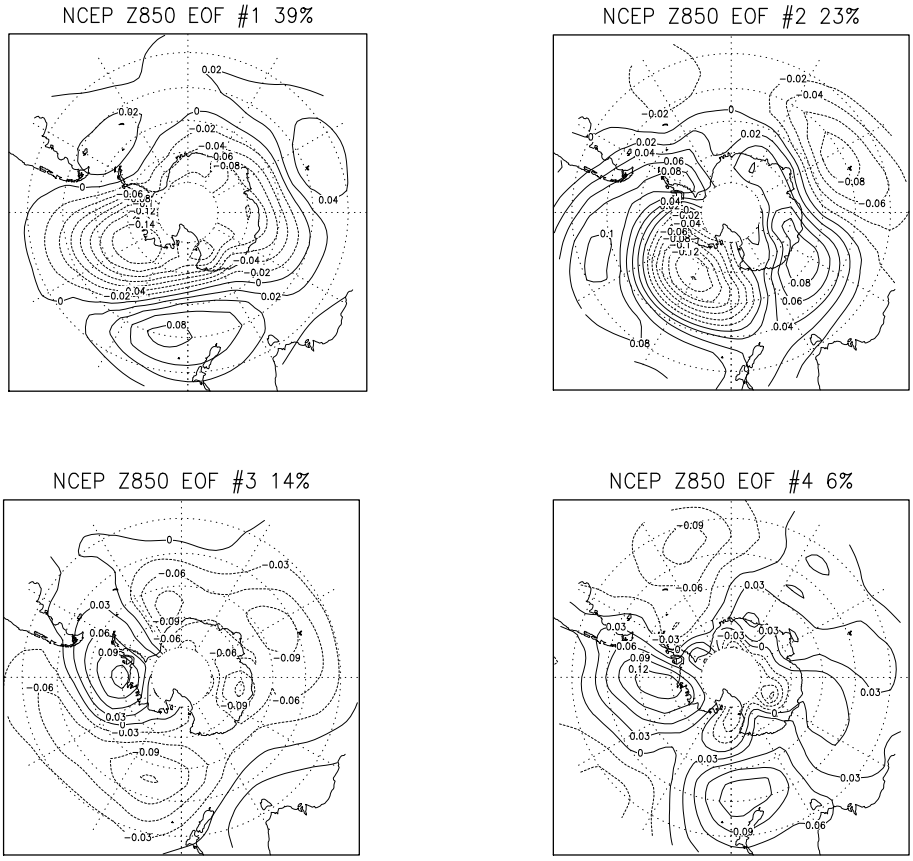
NCEP Z850 EOF #1 39%
NCEP Z850 EOF #2 23%
NCEP Z850 EOF #3 14%
NCEP Z850 EOF #4 6%

Figure 3a

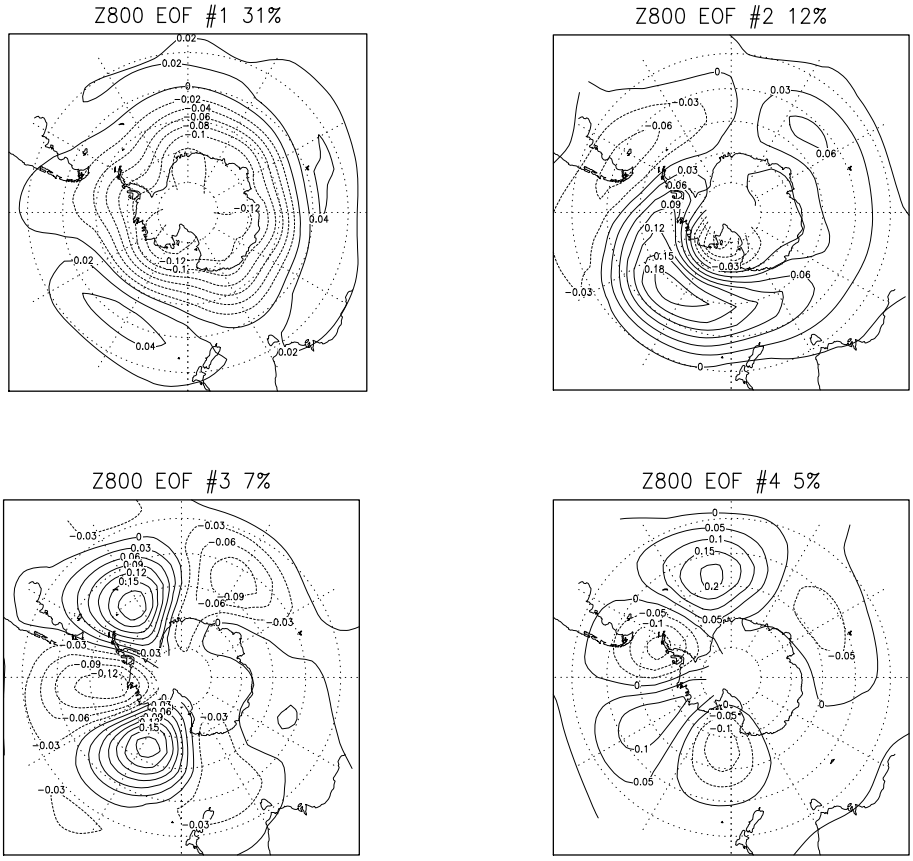

Figure 3b

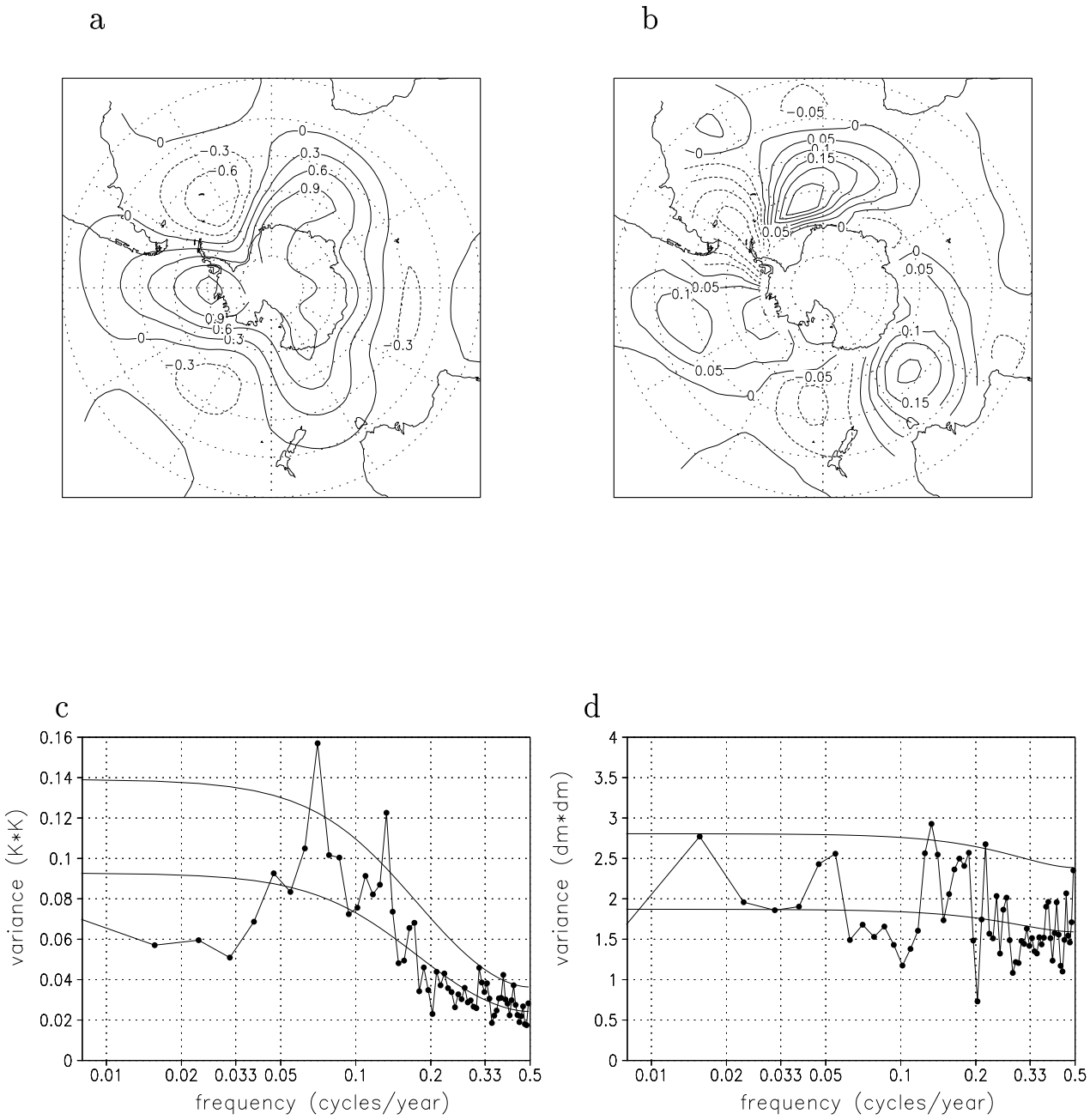
a
b
c
d
variance (K*K)
frequency (cycles/year)
variance (dm*dm)
frequency (cycles/year)
0.01
0.02
0.033
0.05
0.1
0.2
0.33
0.5

Figure 4

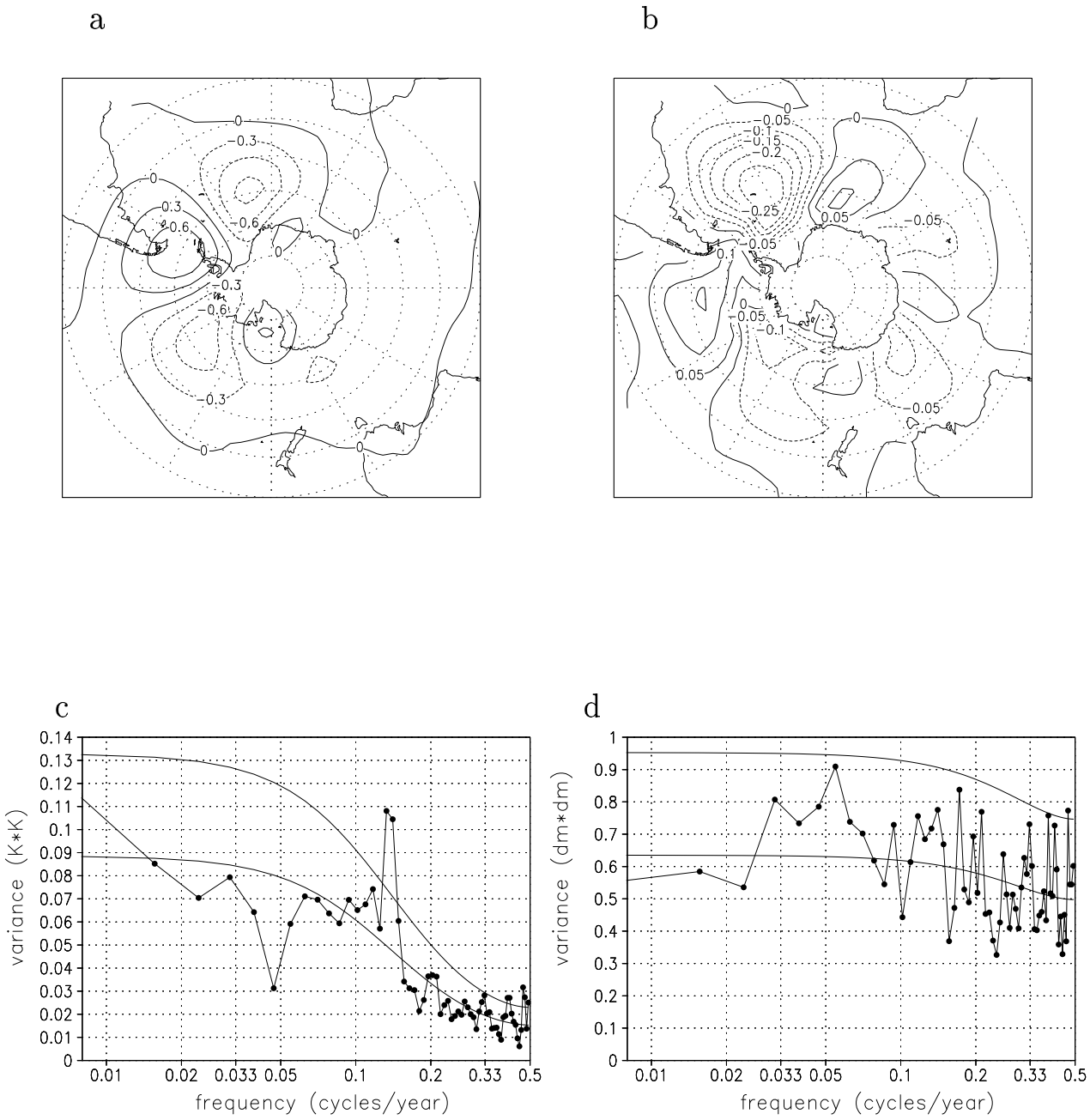
a
b
c
d
variance (K*K)
frequency (cycles/year)
variance (dm*dm)
frequency (cycles/year)

Figure 5

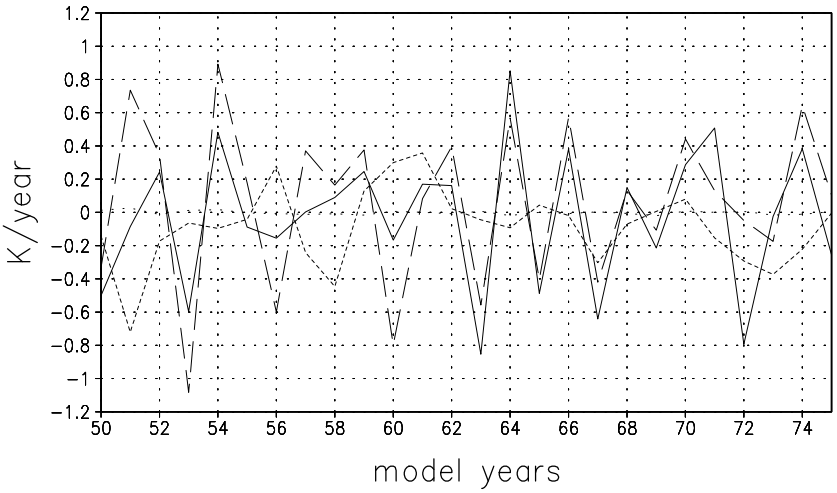
1.2
1
0.8
0.6
0.4
0.2
0
−0.2
−0.4
−0.6
−0.8
−1
−1.2
K/year
50
52
54
56
58
60
62
64
66
68
70
72
74
model years

Figure 6

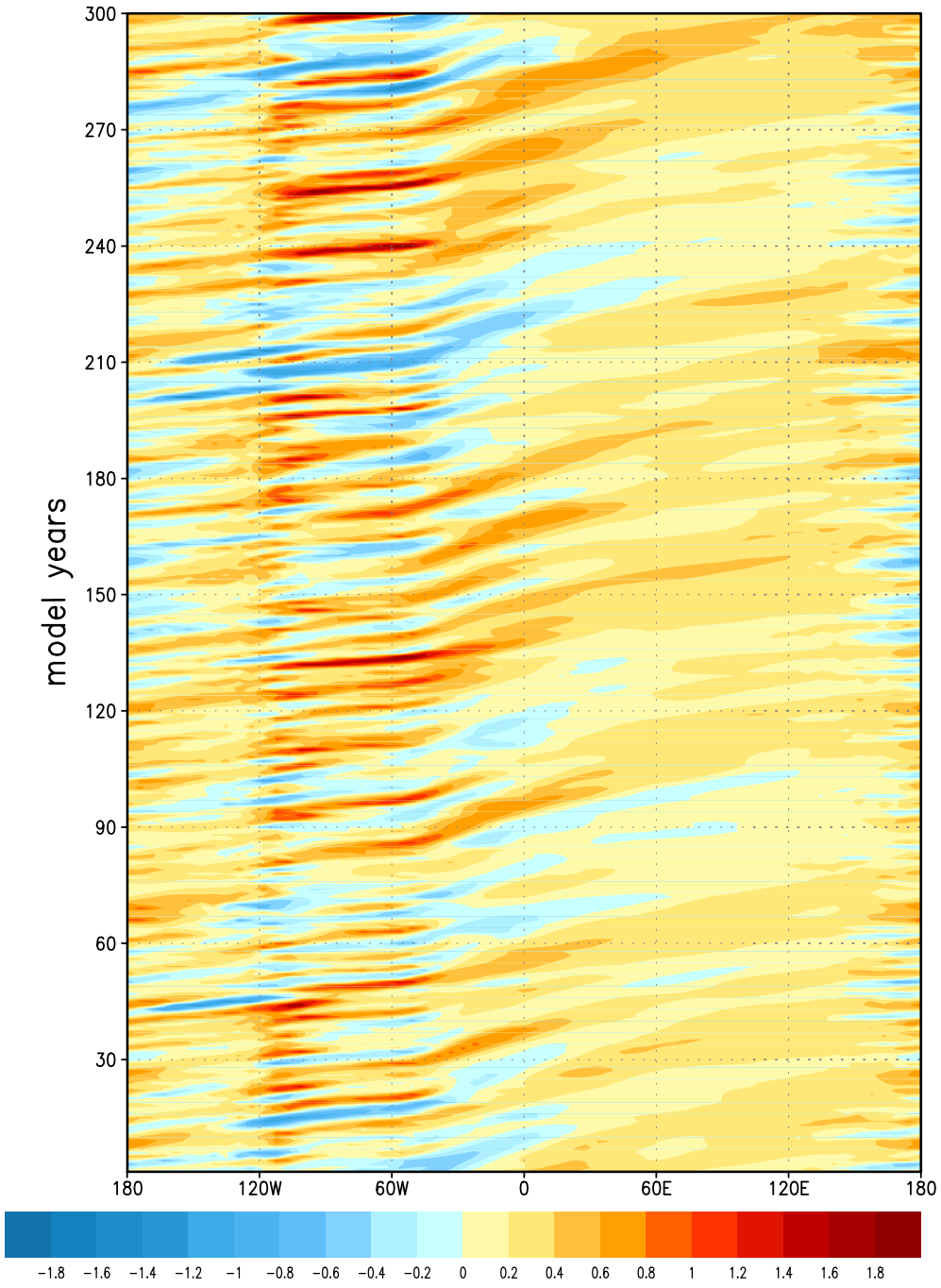
model years
300
270
240
210
180
150
120
90
60
30
180
120W
60W
0
60E
120E
180
−1.8
−1.6
−1.4
−1.2
−1
−0.8
−0.6
−0.4
−0.2
0
0.2
0.4
0.6
0.8
1
1.2
1.4
1.6
1.8

Figure 7

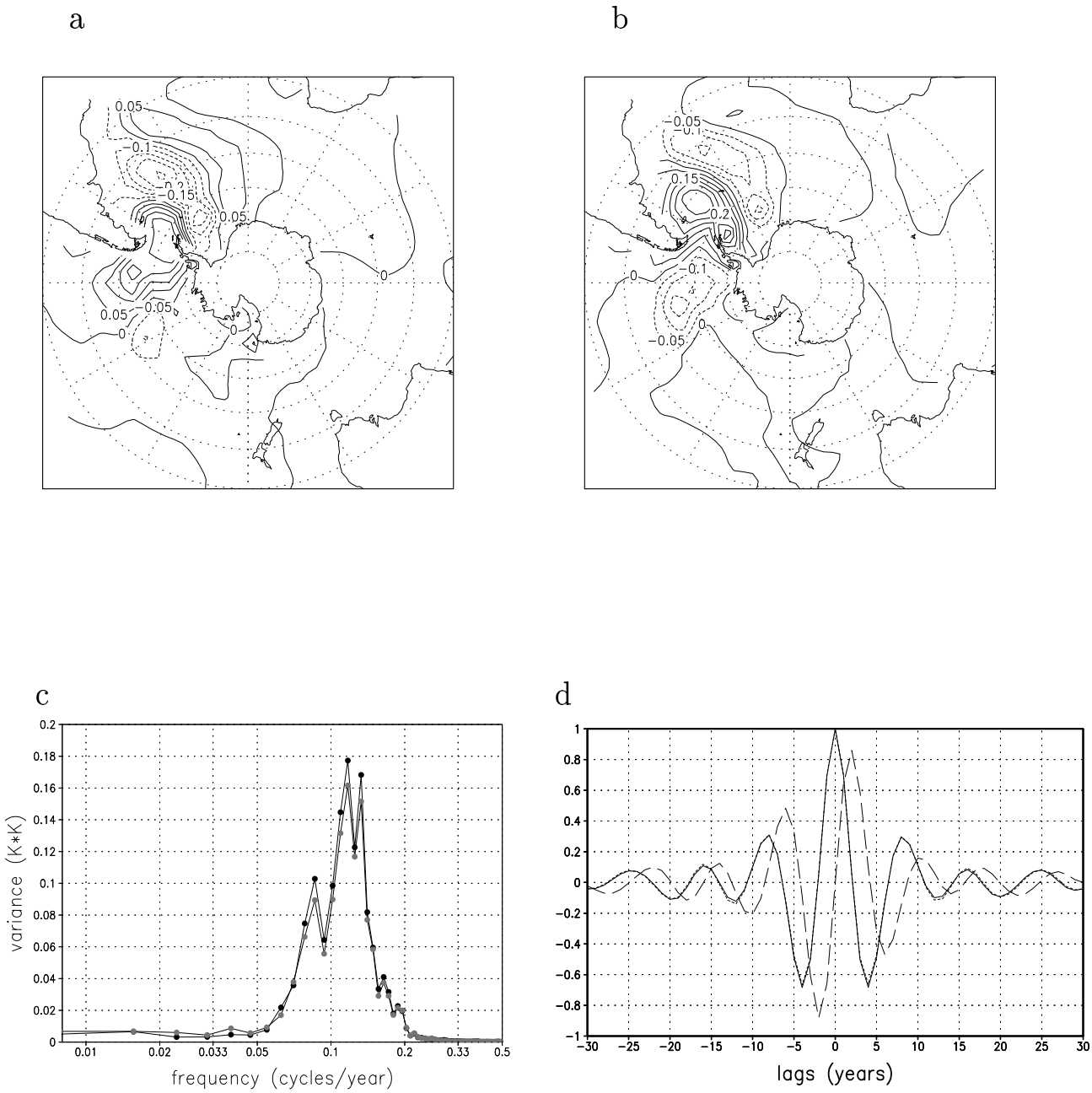
a
b
0.05
−0.1
−0.15
0.05
0
0.05
−0.05
0
0
−0.05
−0.1
0.15
0.2
−0.1
0
−0.05
c
d
variance (K*K)
frequency (cycles/year)
0.01
0.02
0.033
0.05
0.1
0.2
0.33
0.5
lags (years)

Figure 8

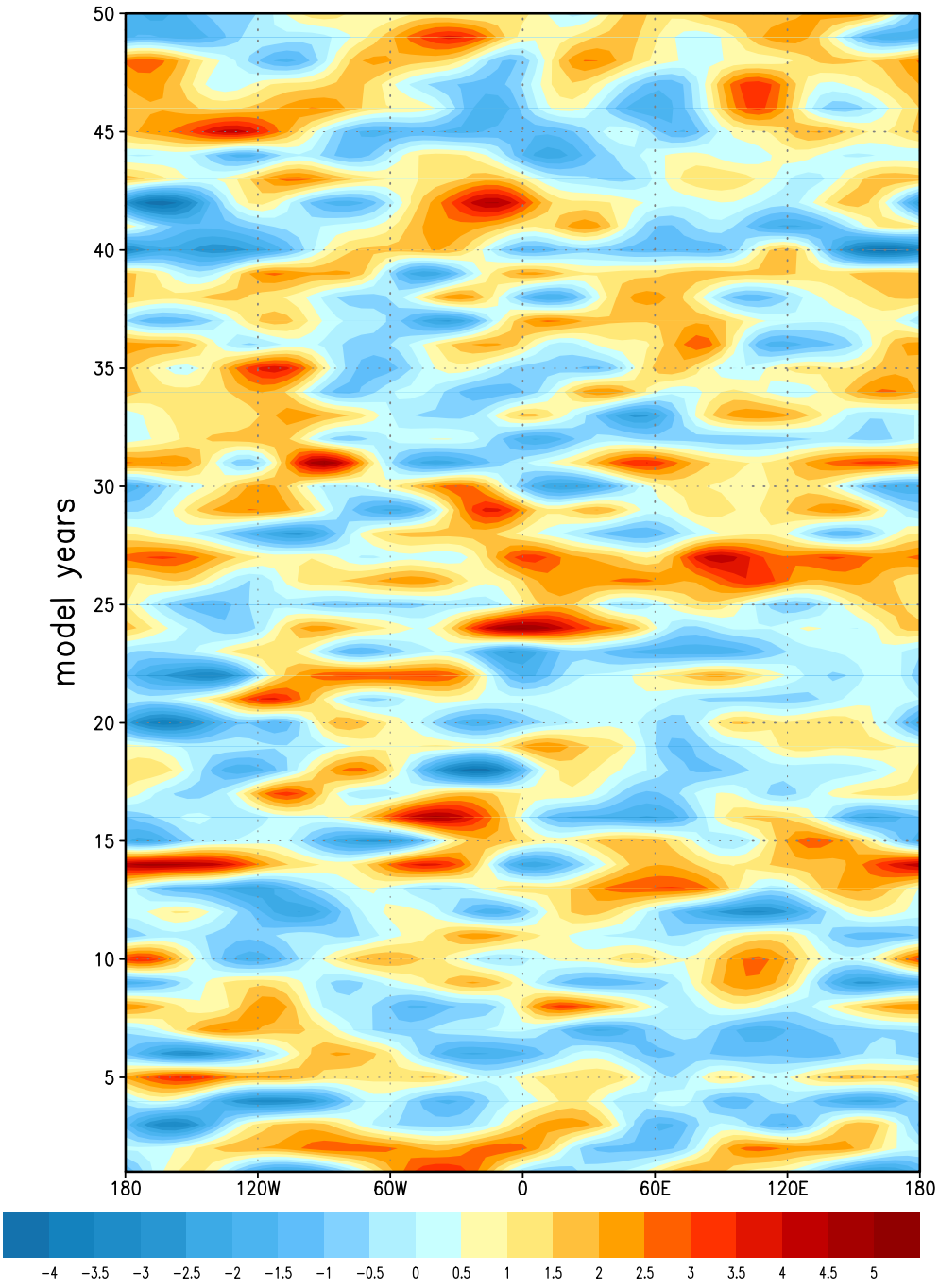
model years
50
45
40
35
30
25
20
15
10
5
180
120W
60W
0
60E
120E
180
−4
−3.5
−3
−2.5
−2
−1.5
−1
−0.5
0
0.5
1
1.5
2
2.5
3
3.5
4
4.5
5

Figure 9

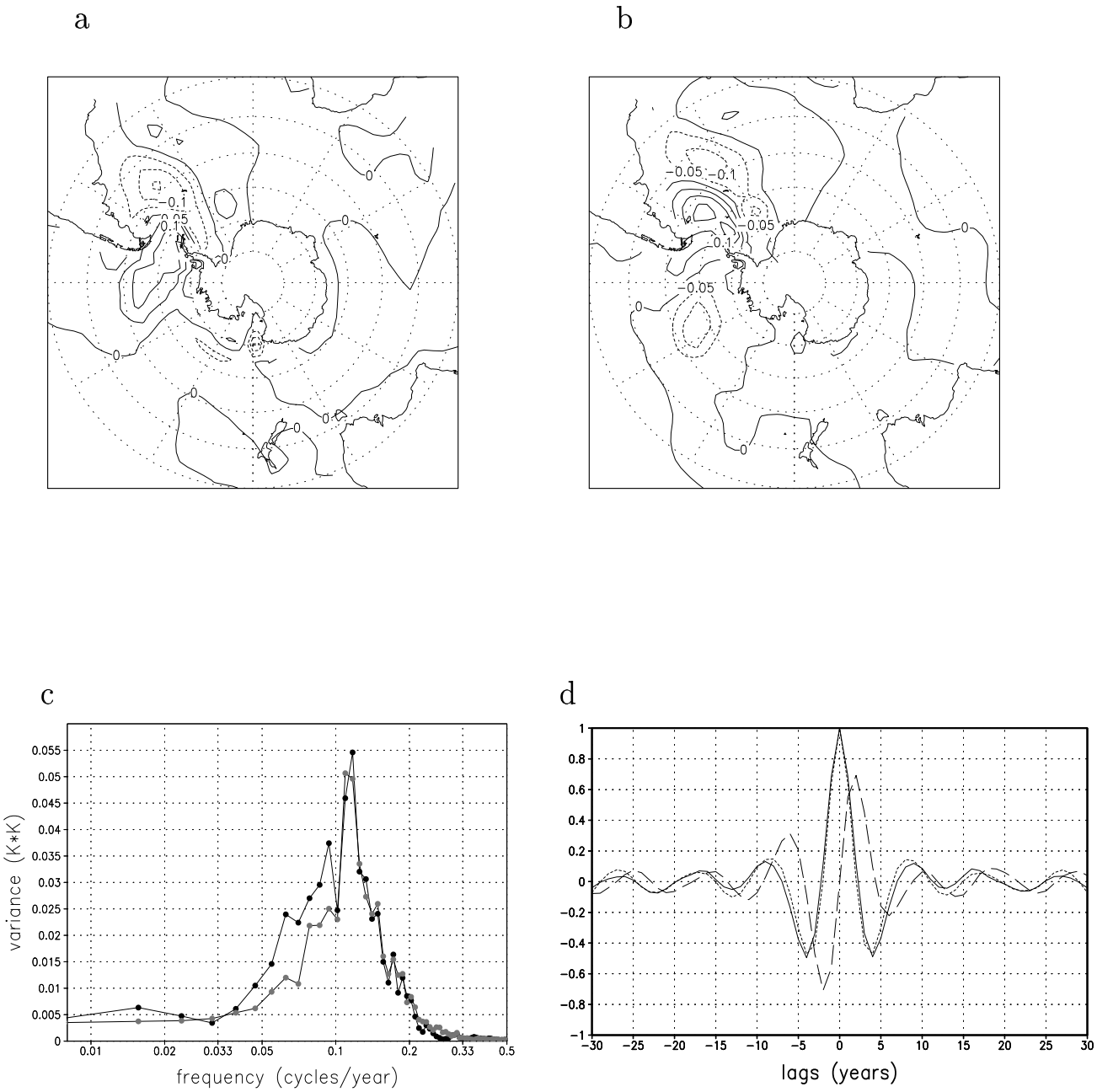
a
b
c
d
−0.1
−0.05
0.1
0
−0.05
−0.1
−0.05
0.1
−0.05
0
variance (K*K)
0.055
0.05
0.045
0.04
0.035
0.03
0.025
0.02
0.015
0.01
0.005
0
0.01
0.02
0.033
0.05
0.1
0.2
0.33
0.5
frequency (cycles/year)
1
0.8
0.6
0.4
0.2
0
−0.2
−0.4
−0.6
−0.8
−1
−30
−25
−20
−15
−10
−5
0
5
10
15
20
25
30
lags (years)

Figure 10

a

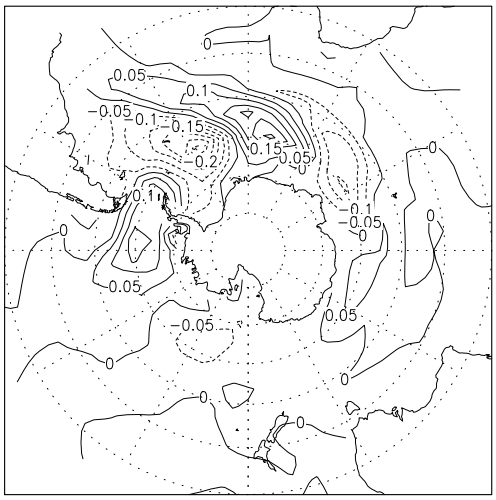

b

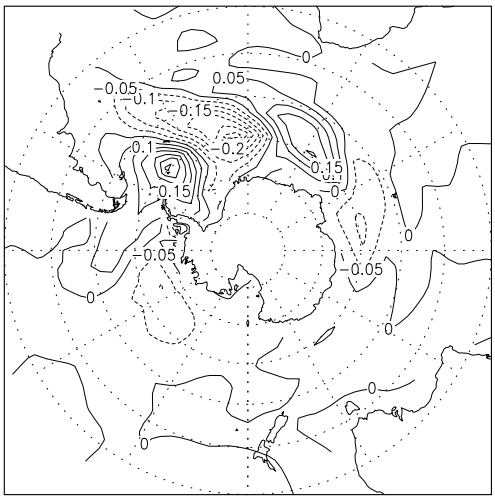

c

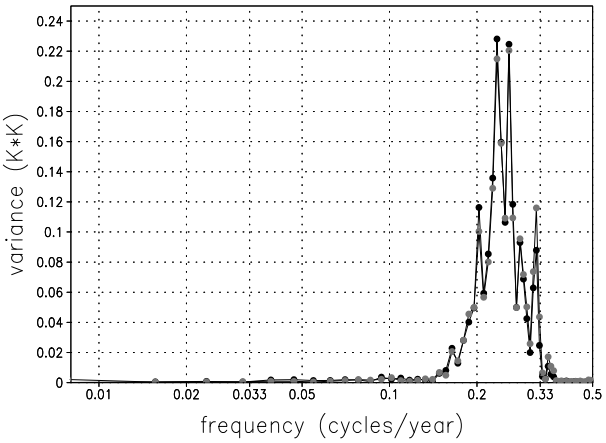

d

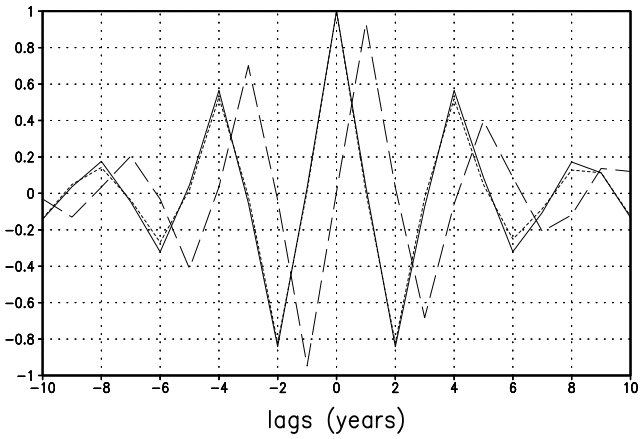

Figure 11

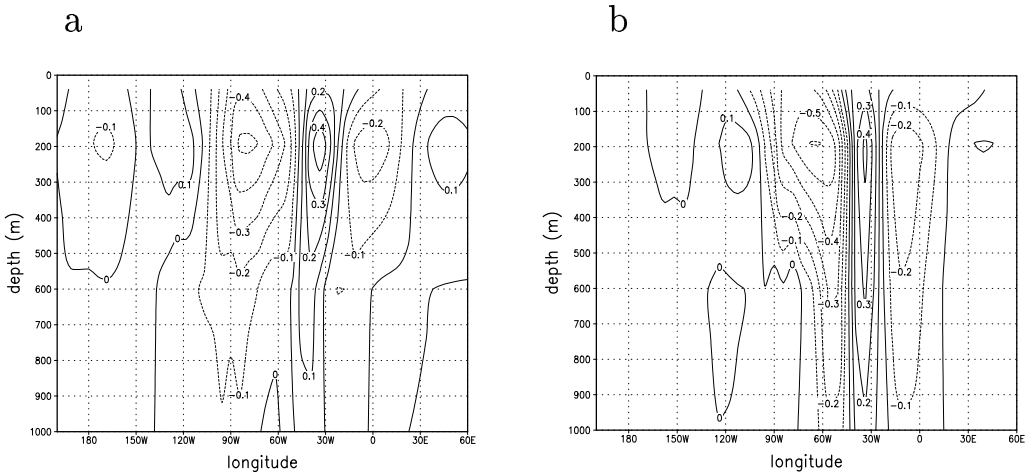
a
b
depth (m)
longitude
0
100
200
300
400
500
600
700
800
900
1000
180
150W
120W
90W
60W
30W
0
30E
60E

Figure 12

a

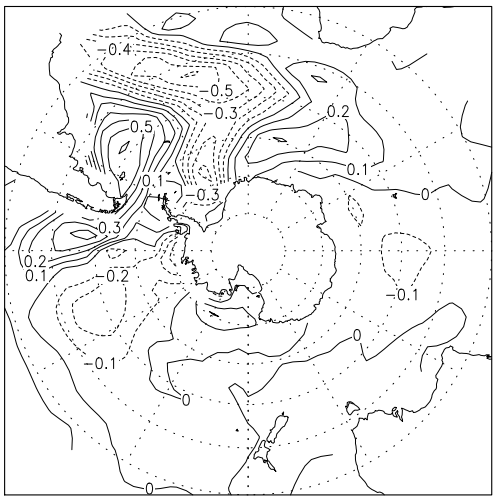
−0.4
−0.5
−0.3
0.2
0.5
0.1
−0.3
0.1
0
−0.3
0.2
0.1
−0.2
−0.1
0
−0.1
0

b

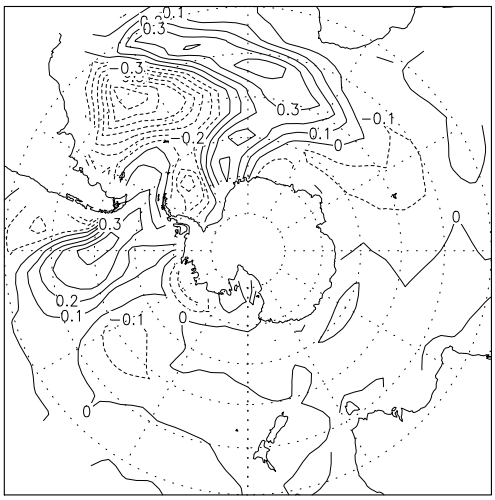
0.1
0.3
−0.3
0.3
−0.1
−0.2
0.1
0
0.3
0
0.2
0.1
−0.1
0
0

Figure 13

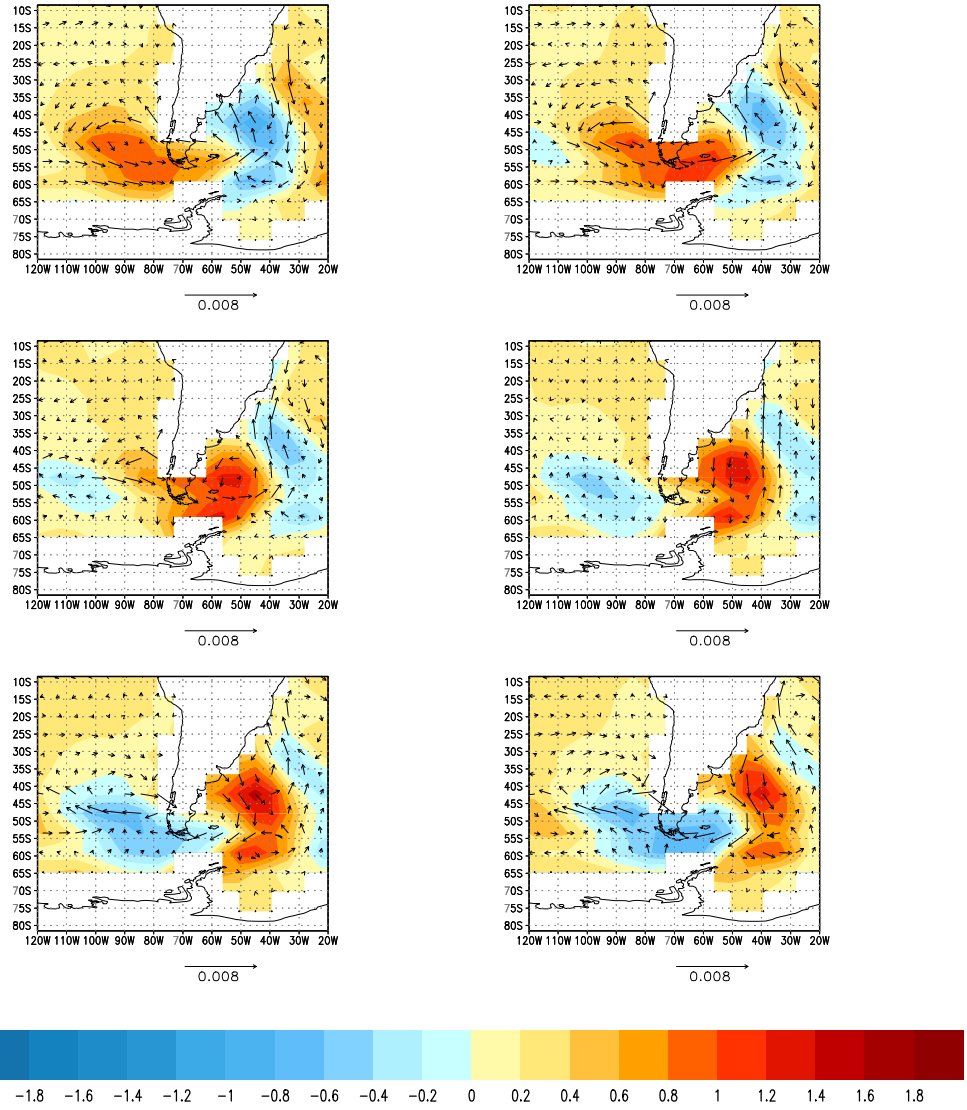
10S
15S
20S
25S
30S
35S
40S
45S
50S
55S
60S
65S
70S
75S
80S
120W 110W 100W 90W 80W 70W 60W 50W 40W 30W 20W
0.008
−1.8 −1.6 −1.4 −1.2 −1 −0.8 −0.6 −0.4 −0.2 0 0.2 0.4 0.6 0.8 1 1.2 1.4 1.6 1.8

Figure 14

a

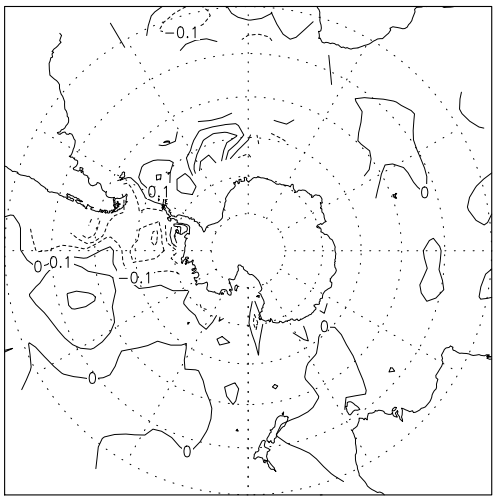

b

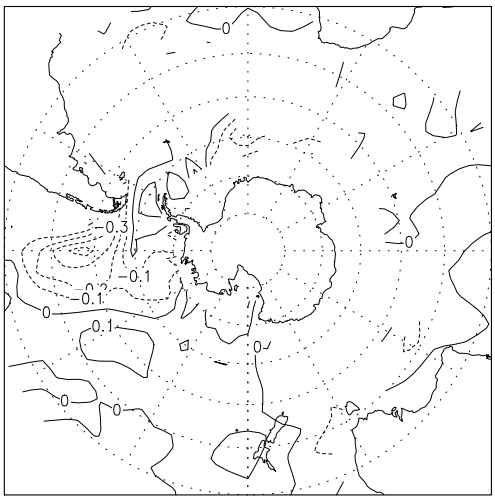

Figure 15

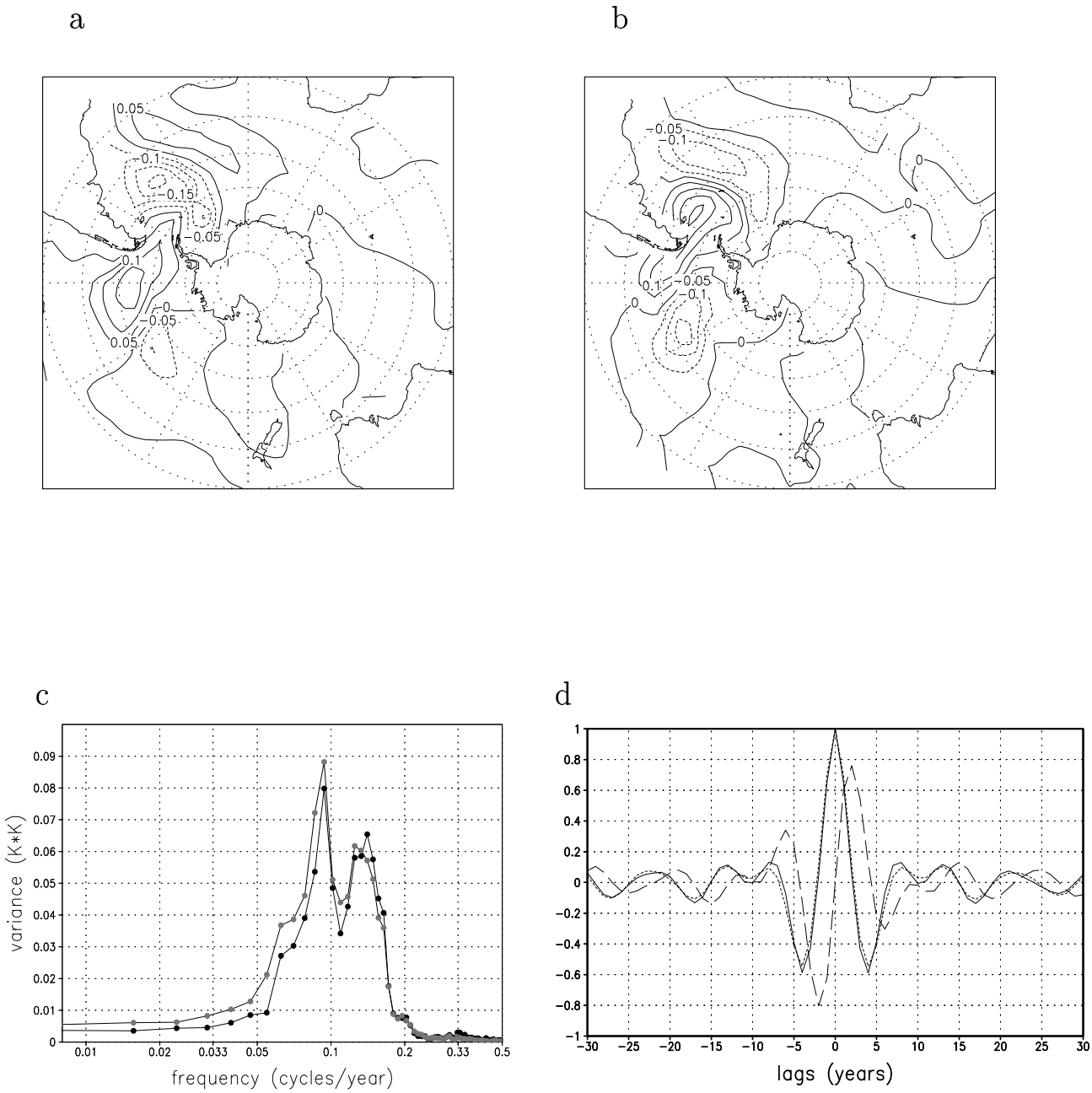
a
b
0.05
−0.1
−0.15
−0.05
0
0.1
−0.05
−0.1
c
d
variance (K*K)
frequency (cycles/year)
0.01
0.02
0.033
0.05
0.1
0.2
0.33
0.5
lags (years)

Figure 16